**American Journal of Naval Architecture and Marine Engineering**
2017; 2(4): 91-98
http://www.sciencepublishinggroup.com/j/ajname
doi: 10.11648/j.ajname.20170204.12

# Numerical Simulation of Scour Depth in Open Channels of Tideland Dike

**Jo Jong-Song**

Faculty of Earth and Environmental Science, Kim Il Sung University, Pyongyang, Democratic People's Republic of Korea

**Email address:**
ryongnam22@yahoo.com

**To cite this article:**
Jo Jong-Song. Numerical Simulation of Scour Depth in Open Channels of Tideland Dike. *American Journal of Naval Architecture and Marine Engineering*. Vol. 2, No. 4, 2017, pp. 91-98. doi: 10.11648/j.ajname.20170204.12

**Received**: July 14, 2017; **Accepted**: August 2, 2017; **Published**: September 4, 2017

**Abstract:** In the present study, the local scour and topographical change in open channels of a tideland dike are studied numerically. A 2D numerical model was presented for the simulation of scour depth in open channels of the tideland dike in the west of the DPR Korea. Because the computation using a 3D numerical model is time-consuming, the depth-averaged 2D numerical model is applied in the calculation of the scour depth. The numerical model is implemented by the method coupled finite element method with finite difference method. Generally, scour depth depends on flow velocity, bed material composition, and suspended sediment concentration. In the present study, as the width of open channel between tideland dikes decreased, the scoured depth dramatically increased due to increased flow velocity. For all the scenarios of damming up, however, the scoured depth increased very slightly in open channels with the width of 50 m. The numerical results showed that when damming up according to Scenario 1, the flow velocity and scoured depth are smallest.

**Keywords:** Dike, Numerical Model, Open Channel, Scour Depth, Tideland

## 1. Introduction

All over the world, the demand for multi-purpose use of tideland areas (coastal areas) have been increased in recent years. In addition, scientific researches on stability of coastal structures and topographies have been carried out with much use of numerical calculation methods, which have progressed significantly, together with hydraulic model and field experiments. Tideland dikes are widely used to protect low-lying areas against floods and to obtain croplands from tideland. As such, they have been widely applied in many coastal countries such as the Netherlands, Thailand, and China.

Especially, dikes have been extensively used for obtaining croplands by reclaiming tideland in the DPR Korea over the past several decades. There are few croplands in the DPR Korea, because mountains account for nearly 80 % of the territory. For this reason, the country has obtained croplands by constructing the tideland dikes in the West Sea of Korea. About ten thousand hectares of the tideland has been reclaimed as croplands for agriculture.

Analysis of a scour depth in open channels of final damming up area due to sediment transport caused by flooding and pressure flow conditions is important for the design, construction and maintenance of dikes. Due to the flood or increased water flow, the scour of the bed in open channels is very common reasons for dam breaks. Under the flooded condition, formation of scour-pit at the open channel bed weakens the strength of dikes, which eventually affects the dike construction. The accurate analysis of this kind of scour in open channels depends on the water flow field, turbulence conditions, and sediment bed forms, along with the interaction between the water and the sediments.

Water flow, sediment transport, and scour problems have been extensively studied numerically by many researchers in the past decades [1-2, 4, 13-15, 19, 21-23, 26, 28-29, 31]. Comer et al. [9] applied multi-scale nested flood (MSN_Flood) model to simulate complex coastal-fluvial urban flooding due to combined effects of tides, surges and river discharges. Cameron et al [6] identified and quantified very-large-scale motions (VLSMs) in rough-bed OCF using long-duration (2 hours) particle image velocimetry (PIV) measurements. Several 2D and 3D numerical models with the capability of predicting scour depths have been reported in many studies. Guo [16] modified the Shields-Rouse equation for the evaluation of critical shear stress based on the experimental results. Smith [25] reported the modeling

technique of a contraction scour around a cylinder by using volume-of-fraction (VOF) methodology. Vikas [28] studied an integrated two-dimensional sediment transport model for simulating the sediment transport in water medium. Both the bed load and suspended load have been taken into account in this work. Acharya [1] studied experimentally and simulated numerically flow and sediment transport around a series of spur dikes. He used a three-dimensional numerical model FLOW-3D to simulate the turbulent flow field around a series of spur dikes in flat and scoured bed. In the dissertation, he examined Prandtl's mixing length model, one equation model, standard two-equation k-ε model, Renormalization-Group (RNG) k-ε model, and Large Eddy Simulations (LES) turbulence model. Roulund et al. [24] investigated the flow velocity and the scour depth around a bridge pier both experimentally and numerically. He used a finite volume method and calculated the turbulence with the k-ω model. A free-surface algorithm was not used in their study. Coleman et al. [7] analyzed clear-water scour development at bridge abutments and Dey [13] studied experimentally threshold of sediment motion on combined transverse and longitudinal sloping beds. Zhihe and Fernedo [31] carried out CFD simulation for the evolution of scour around pipelines. They analyzed the effect of different sediment transport modes, such as bed-load, and suspended-load on the development of scour. Duc and Rodi [14] simulated numerically contraction scour in an open laboratory channel. Afzal [2] studied 3D numerical model of sediment transport under current and waves. He used the level set method for the calculation of the complex free surface and for the representation of the moveable sediment bed. Bihs and Olsen [4] performed numerical simulations of pier scour. Good agreement was found with the physical model studies. Later, they focused on the influence of the sloping bed in scour holes (Bihs and Olsen [5]). Mortlock et al. [20] studied the coastal erosion risk by using A MIKE 21/3 Coupled Model developed by the Danish Hydraulic Institute (DHI). The primary focus of their study was to demonstrate the importance of storm wave direction for coastal erosion impacts. For the simulation of bedload transport, Török et al. [26] presented the combined application of two bedload transport formulas. To gain a deeper understanding of the scouring process near embankment foundations, Guo et al. [17] proposed a straightforward and practical method for bend scour simulation.

Generally, an accurate prediction of scour depth and its evolution is decisive. Therefore, extensive experience and physical insight into the hydrodynamics and sediment transport is necessary. The objective of this study is to develop a simulation model to predict the bed depths scoured in open channels of final damming up area. Also, it is considered to select a reasonable scenario for final damming up according to the scoured bed depths. For this purpose, an integrated two-dimensional numerical model is proposed and tested.

## 2. Case Studied

This section gives the outline of the study area. To start the research, the focus is tightened to a tideland area where dikes are being built up in west coast of the DPR Korea (Figure 1). A schematic geometry of the tideland area is used to make the tideland model.

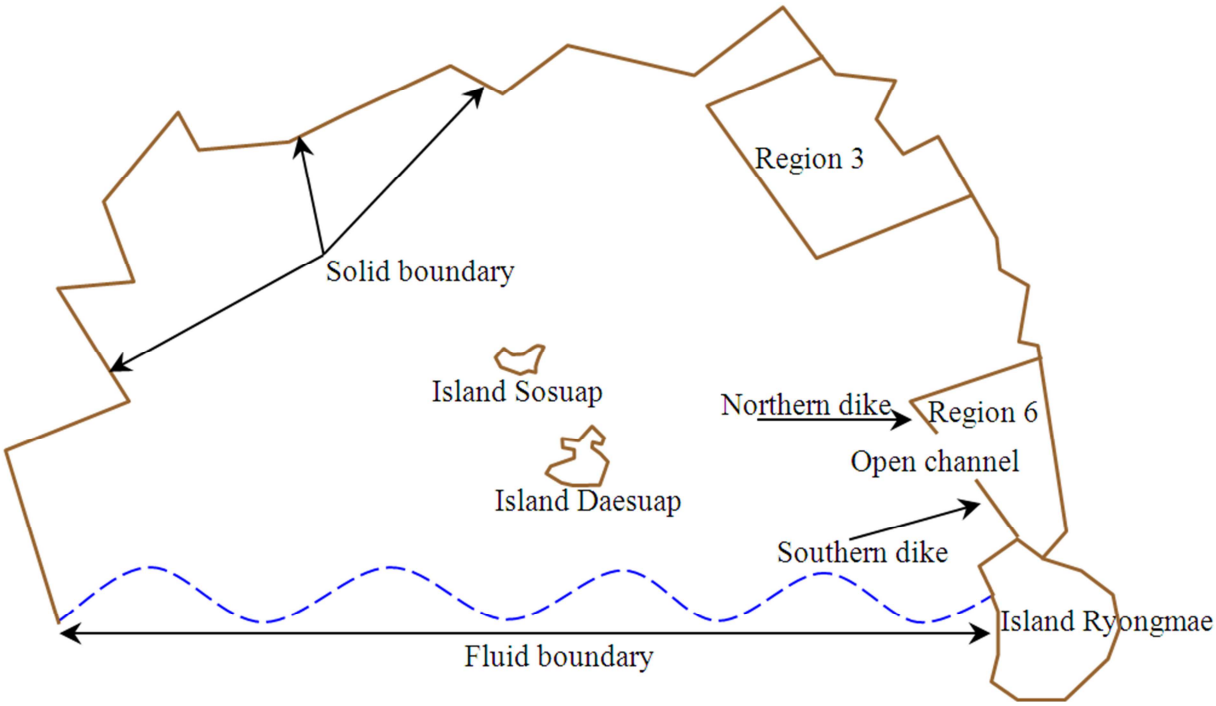


***Figure 1.*** *(Color online) Dike geometry and boundary conditions.*

The simulated tideland area includes the region 3 enclosed already with dikes, island Daesuap, and island Sosuap. The area of the region 3 is about 3600 hectares. The region 6 enclosing with dikes is also included in the study area. The area of the region 6 to be enclosed is about 4500 hectares. The region 6 is focus of the present study for the simulation of the flow velocity and the scour depth. The northern dike was built up to 1153 m and southern dike was built up to 3192 m. The distance between the ends of these two dikes (i.e. the width of open channel) is about 880 m at present. In the present study, the open channel is referred to as final damming up area. The tideway of 250 m in width was already made on the end of southern dike and the depth of deepest place of the tideway is about 6.5 m. As shown in Figure 1, the simulated tideland area bounds fluid and solid regions. To simulate the depth scoured in different open channels, three different scenarios were designed and simulated as follows: Scenario 1 was to dam up from the end of northern dike toward the south. Scenario 2 was to dam up from the end of southern dike toward the north. Scenario 3 was to dam up simultaneously face to face from each other.

The primary characteristic of the tideland area on the west coast of Korea is the influence of tides. The tides are semi-diurnal and have an average range of 6.17 m during spring tide and 3.01 m during neap tide. The average flood time is 6.2 hours and the ebb time is 6.15 hours.

# 3. Mathematical Formulation

Generally, sediment transport affects significantly the scour of open channel bed. Sediment transport is controlled by gravity, and drag forces between the sediment and surrounding water. Sediment transport depends on characteristics of bed material, sediment properties, and properties of the flow. It is very difficult to simulate accurately sediment transport and scour depth due to many such factors. Therefore, general assumptions are absolutely necessary. In the present study, there were assumptions as follows:

(a) The fluid is incompressible.

(b) The pressure distribution is hydrostatic.

(c) Vertical accelerations can be neglected if a flow is shallow enough.

(d) The influences of wind and wave are neglected.

### *3.1. Governing Equations*

The following 2-D governing equations, the conservation of mass and momentum integrated over the vertical, describe the flow velocity, sediment concentration, and scour depth variations:

$$\frac{\partial z}{\partial t}+\frac{\partial}{\partial x}(Hu)+\frac{\partial}{\partial y}(Hv)=0 \tag{1}$$

$$\frac{\partial u}{\partial t}+u\frac{\partial u}{\partial x}+v\frac{\partial u}{\partial y}-Fv+g\frac{\partial z}{\partial x}+\frac{guW}{c^2H}=0 \tag{2}$$

$$\frac{\partial v}{\partial t}+u\frac{\partial v}{\partial x}+v\frac{\partial v}{\partial y}+Fu+g\frac{\partial z}{\partial y}+\frac{gvW}{c^2H}=0 \tag{3}$$

$$\frac{\partial s}{\partial t}+\frac{\partial (us)}{\partial x}+\frac{\partial (vs)}{\partial y}=\frac{d\omega}{H} \tag{4}$$

$$\gamma\frac{\partial z_0}{\partial t}=-\alpha\omega(\beta_1 s_x-\beta_2 s) \tag{5}$$

Where, $x$, $y$ = space coordinates; $u$, $v$ = average velocity components in 2 orthogonal directions $x$, $y$; $t$ = time; $z$ = time varying water depth; $H$ = surface elevation; $F$ = Coriolis parameter; $c$ = Chezy resistance; $W=\sqrt{u^2+v^2}$; $s$ = depth averaged mass concentration; $s_x$ = saturated mass concentration (transport capacity of flow); $\alpha$ = settling probability of sediment; $\omega$ = settling velocity of sediment; $\gamma$ = density of dry bed material; $g$ = acceleration due to gravity; $z_0$ = initial thickness of bed material.

$$\beta_1=\begin{cases}1, W\geq u_c\\ 0, W<u_c\end{cases},$$

$$\beta_2=\begin{cases}1, W\geq u_f\\ 0, W<u_f\end{cases}.$$

Where, $u_c$ = critical flow velocity for sediment transport; $u_f$ = critical flow velocity for sediment suspension.

The formulas for the calculation of $\omega$, $s_x$, $u_c$, and $u_f$ according to the diameter of sediment $d$ were already studied experimentally. For example, when $d$ < 0.05 mm, the formulas are as follows:

$$\omega=90.0\frac{d^2}{v} \quad \text{or} \quad \omega=\frac{(\rho_s-\rho)gd^2}{18\mu},$$

$$s_x=0.027\,3\rho\frac{W^2}{gH},$$

$$u_c=(H/d)^{0.14}\left(17.6\frac{\rho_s-\rho}{\rho}\cdot d+6.05\cdot 10^{-7}\frac{10+H}{d^{0.72}}\right)^{1/2},$$

$$\text{and} \quad u_f=0.812d^{2/5}\cdot\omega^{1/5}\cdot H^{1/5}.$$

Where, $\rho_s$ = density of sediment; $\rho$ = density of water.

### *3.2. Initial Conditions*

At the first time step, the initial water level at the inlet

boundary (fluid boundary) is 4.1 m, the initial flow is 0 m/s in all the direction, the initial sediment concentration is 0 g/m$^3$, and the initial scoured depth is 0 m.

$$z(x,\ y,\ 0) = z_{fluid\ boundary}(x,\ y) = 4.1\ m\ ,$$

$$u(x,\ y,\ 0) = v(x,\ y,\ 0) = 0\ ,$$

$$s(x,\ y,\ 0) = s_0(x,\ y) = 0\ ,$$

$$\text{and}\quad z_0(x,\ y,\ 0) = 0\ .$$

### *3.3. Boundary Conditions*

#### *3.3.1. Solid Boundary*

$$u(x,\ y,\ t) = v(x,\ y,\ t) = 0 \quad \text{or} \quad W_n = 0\ ,$$

$$\text{and}\quad \frac{\partial s}{\partial n} = 0\ .$$

#### *3.3.2. Fluid Boundary*

In the fluid boundary, the variation of the water level is formulated by the following formula:

$$z_{fluid\ boundary}(x,\ y,\ t) = z_i + \frac{z_{i+1} - z_i}{2}\left[1 - \cos\left(\frac{t - T_i}{T_{i+1} - T_i}\cdot\pi\right) - G\right] \quad (6)$$

Where $T_i$ = time of high tide or low tide; $z_i$ = level of high tide or low tide; $t$ = simulated time; $G$ = initial phase angle of flow.

When flow into the domain (study area), $s(x,\ y,\ t) = s_{fluid\ boundary}(x,\ y,\ t)$ . When flow out the domain (study area),

$$\frac{\partial s}{\partial t} + \frac{\partial (us)}{\partial x} + \frac{\partial (vs)}{\partial y} = 0$$

### *3.4. Stability Condition*

Stability is controlled mainly by the value of $\Delta t$ . The requirement is the Courant number condition:

$$\Delta t \le (1 - \alpha)\frac{\Delta x}{\sqrt{2gh}_{\max}} \quad (\alpha \ge 0.4)$$

Where, $h_{\max}$ is the maximum depth of flow.

## 4. Numerical Model

In the past, many researchers studied numerical models for solving governing equations 1–5 [3, 8, 10–12, 18, 23, 27, 32–34]. In the present study, the method coupled finite element method with finite difference method was used. The two-dimensional equations are discretized by the coupled method as follows.

$$z_i^{n+1} = z_i^n - \Delta t\left\{\left(\frac{\partial}{\partial x}[Hu]\right)_i^n + \left(\frac{\partial}{\partial y}[Hv]\right)_i^n\right\} \quad (7)$$

$$u_i^{n+1} = \left\{u_i^n - \Delta t\left[v_i^n\left(\frac{\partial u}{\partial y}\right)_i^n + g\left(\frac{\partial z}{\partial x}\right)_i^{n+1} - Fv_i^n\right]\right\} \Bigg/ \left\{1 + \Delta t\left[\left(\frac{\partial u}{\partial x}\right)_i^n + g\frac{W_i^n}{c_i^2 H_i^{n+1}}\right]\right\} \quad (8)$$

$$v_i^{n+1} = \left\{v_i^n - \Delta t\left[u_i^n\left(\frac{\partial v}{\partial x}\right)_i^n + g\left(\frac{\partial z}{\partial y}\right)_i^{n+1} + Fu_i^n\right]\right\} \Bigg/ \left\{1 + \Delta t\left[\left(\frac{\partial u}{\partial y}\right)_i^n + g\frac{W_i^n}{c_i^2 H_i^{n+1}}\right]\right\} \quad (9)$$

$$s_i^{n+1} = s_i^n - \Delta t\left\{\left(\frac{\partial}{\partial x}[us]\right)_i^n + \left(\frac{\partial}{\partial y}[vs]\right)_i^n - \frac{\alpha\omega}{H_i^n}(\beta_1 s_{xi}^n - \beta_2 s_i^n)\right\} \quad (10)$$

$$z_{0i}^{n+1} = z_{0i}^n - \frac{\alpha\omega\Delta t}{\gamma}(\beta_1 s_{xi}^{n+1} - \beta_2 s_i^{n+1}) \quad (11)$$

Where, the terms $(\ )_i^n$ of models 6–10 are calculated as follows.

If $z$ , $u$ , $v$ , and $s$ is represented as function $f$ ,

$$\left.\begin{aligned}\left(\frac{\partial f}{\partial x}\right)_i^n &= \sum_{i=1}^{m} D_l / A_i \\ \left(\frac{\partial f}{\partial y}\right)_i^n &= \sum_{i=1}^{m} E_l / A_i\end{aligned}\right\} \quad (12)$$

$$A_i = \sum_{i=1}^{m} e_l \tag{13}$$

Where, $m$ = number of elements owned the point $i$ jointly; $e_l$ = area of $l^{th}$ element.

$$\left.\begin{aligned} D_l &= \left[b_3(c_1+c_2)-b_2(c_3+c_4)\right]_l \\ E_l &= \left[-a_3(c_1+c_2)+a_2(c_3+c_4)\right]_l \end{aligned}\right\} \tag{14}$$

Where,

$$\left.\begin{aligned} a_2 &= (-x_1+x_2+x_3-x_4)/4 \\ a_3 &= (-x_1-x_2+x_3+x_4)/4 \end{aligned}\right\} \tag{15}$$

$$\left.\begin{aligned} b_2 &= (-y_1+y_2+y_3-y_4)/4 \\ b_3 &= (-y_1-y_2+y_3+y_4)/4 \end{aligned}\right\} \tag{16}$$

$$\left.\begin{aligned} c_1 &= f_2^n - f_1^n,\ c_2 = f_3^n - f_4^n \\ c_3 &= f_4^n - f_1^n,\ c_4 = f_3^n - f_2^n \end{aligned}\right\} \tag{17}$$

## 5. Calculation Procedure

The governing equations are the two-dimensional momentum and continuity, the sediment transport equation, and the bed thickness change equation. In summary, the calculation procedure is as follows:

(1) Setting the initial conditions.

(2) Setting the boundary conditions.

(3) Computing the water level and flow velocity.

(4) Computing $\omega$, $u_c$, $u_f$, $s_x$.

(5) Computing $s_i^{n+1}$.

First, $c_1 - c_4$ are computed by solving the equation (17) and $E$ and $D$ are computed by solving the equation (14).

Next, the differential terms are computed by solving the equation (12).

Finally, $s_i^{n+1}$ is computed by solving the equation (10).

(6) Computing $z_{0i}^{n+1}$ by solving the equation (11).

## 6. Results and Discussion

Considering the characteristic of study area, the depth averaged mass concentration $s$ was 200 $mg/m^3$ and the density of dry bed material was 1.38 $t/m^3$. The simulated time was 72 $h$ (3 days) with the time step interval of 60 $s$.

### *6.1. Simulated Results of the Flow Velocity and the Scour Depth According to All the Scenarios for Damming up*

For all the scenarios, when the widths of open channel are 600, 550, 500, 450, 400, 350, 300, 250, 200, 150, 100, and 50 m, respectively, the flow velocities and the scoured depths in the open channels are shown below.

#### *6.1.1. Scenario 1*

For scenario 1, the velocity profiles for different widths of open channel are given in Table 1.

***Table 1.*** *Change in the maximum flow velocity in the open channels.*

| Width of open channel (m) | 600 | 550 | 500 | 450 | 400 | 350 | 300 | 250 | 200 | 150 | 100 | 50 |
|---|---|---|---|---|---|---|---|---|---|---|---|---|
| Flow velocity (m/s) | 2.12 | 2.42 | 2.68 | 3.02 | 3.32 | 3.59 | 3.86 | 4.25 | 4.46 | 5.07 | 5.64 | 5.68 |

It is seen that as the width of open channel decreases, the maximum velocity increases almost linearly (average velocity differences of approximately 0.352 m/s). The rise in the maximum velocity represented an across-the-board increase of between 2.12 m/s for the width of 600 m and 5.64 m/s for the width of 100 m. However, the velocity in the open channel with 50 m width increases very slightly than those in other open channels (average velocity difference of approximately 0.04 m/s).

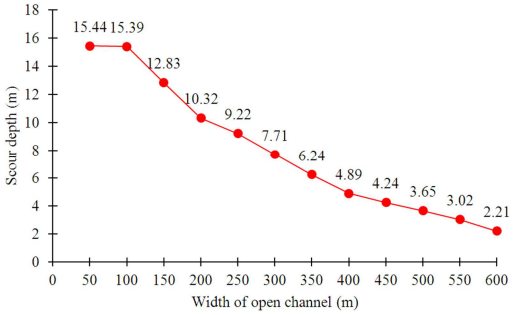


***Figure 2.*** *(Color online) Change in the maximum depth scoured in the open channels according to the maximum flow velocity.*

For scenario 1, the scour profiles for different widths of open channel have been plotted in Figure 2. As shown in Figure 2, the scour profiles are very similar to the flow velocity profiles. The rise in the maximum scour depth represented an across-the-board increase of between 2.21 m for the width of 600 m and 15.39 m for the width of 100 m (average scour depth differences of approximately 1.318 m). However, the scour depth in the open channel with 50 m width increases very slightly than those in other open channels (average scour depth difference of approximately 0.05 m).

#### *6.1.2. Scenario 2*

For scenario 2, the velocity profiles for different widths of open channel are given in Table 2.

It is seen that as the width of open channel decreases, the maximum velocity increases almost linearly (average velocity differences of approximately 0.337 m/s). The rise in the maximum velocity represented an across-the-board increase of between 2.61 m/s for the width of 600 m and 6.01 m/s for the width of 100 m. However, the velocity in the open channel with 50 m width increases very slightly than

those in other open channels (average velocity difference of approximately 0.03 m/s).

***Table 2.*** *Change in the maximum flow velocity in the open channels.*

| Width of open channel (m) | 600 | 550 | 500 | 450 | 400 | 350 | 300 | 250 | 200 | 150 | 100 | 50 |
|---|---|---|---|---|---|---|---|---|---|---|---|---|
| Flow velocity (m/s) | 2.61 | 2.96 | 3.27 | 3.60 | 3.92 | 4.21 | 4.49 | 4.78 | 5.03 | 5.52 | 5.98 | 6.01 |

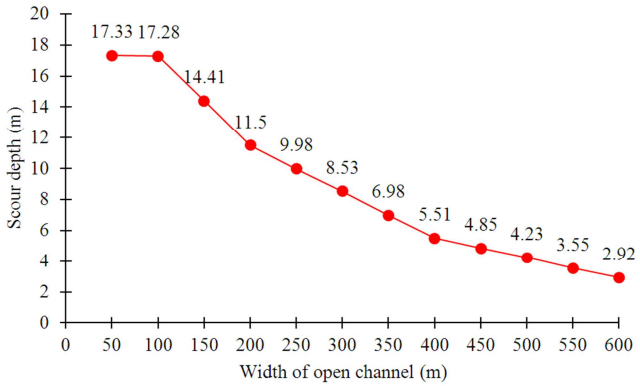


***Figure 3.*** *(Color online) Change in the maximum depth scoured in the open channels according to the maximum flow velocity.*

For scenario 2, the scour profiles for different widths of open channel have been plotted in Figure 3. As shown in Figure 3, the scour profiles are very similar to the flow velocity profiles. The rise in the maximum scour depth represented an across-the-board increase of between 2.92 m for the width of 600 m and 17.28 m for the width of 100 m (average scour depth differences of approximately 1.291 m). However, the scour depth in the open channel with 50 m width increases very slightly than those in other open channels (average scour depth difference of approximately 0.05 m).

### *6.1.3. Scenario 3*

For scenario 3, the velocity profiles for different widths of open channel are given in Table 3.

***Table 3.*** *Change in the maximum flow velocity in the open channels.*

| Width of open channel (m) | 600 | 550 | 500 | 450 | 400 | 350 | 300 | 250 | 200 | 150 | 100 | 50 |
|---|---|---|---|---|---|---|---|---|---|---|---|---|
| Flow velocity (m/s) | 2.46 | 2.71 | 2.99 | 3.23 | 3.52 | 3.82 | 4.15 | 4.46 | 4.78 | 5.18 | 5.62 | 5.69 |

It is seen that as the width of open channel decreases, the maximum velocity increases almost linearly (average velocity differences of approximately 0.316 m/s). The rise in the maximum velocity represented an across-the-board increase of between 2.46 m/s for the width of 600 m and 5.69 m/s for the width of 100 m. However, the velocity in the open channel with 50 m width increases very slightly than those in other open channels (average velocity difference of approximately 0.07 m/s).

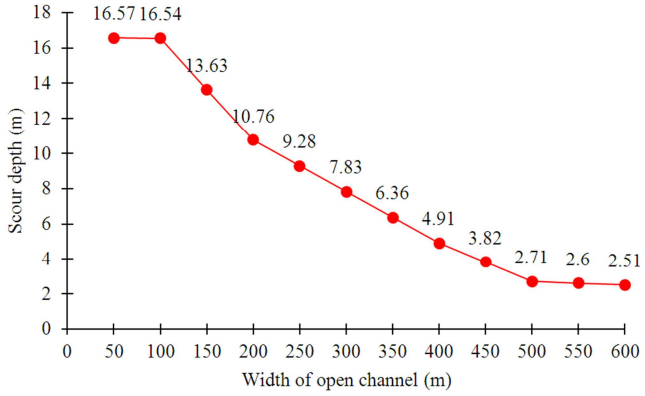


***Figure 4.*** *(Color online) Change in the maximum scoured depth in the open channels according to the maximum flow velocity.*

For scenario 3, the scour profiles for different widths of open channel have been plotted in Figure 4. As shown in Figure 4, the scour profiles are very similar to the flow velocity profiles. The rise in the maximum scour depth represented an across-the-board increase of between 2.51 m for the width of 600 m and 16.54 m for the width of 100 m (average scour depth differences of approximately 1.403 m). However, the scour depth in the open channel with 50 m width increases very slightly than those in other open channels (average scour depth difference of approximately 0.03 m).

### *6.2. Validation of Coupled Model*

For validation of 2D numerical simulation by using the coupled model, the velocity profile across the width of an open channel is measured by an acoustic Doppler current profiler (ADCP) and compared with the numerical results. The width of the channel was 880 m. The average velocity profiles along the width of the open channel obtained from ADCP measurement and the numerical simulation, respectively, are shown in Fig. 5. It is seen that the two velocity profiles are very similar and are lying very close to each other.

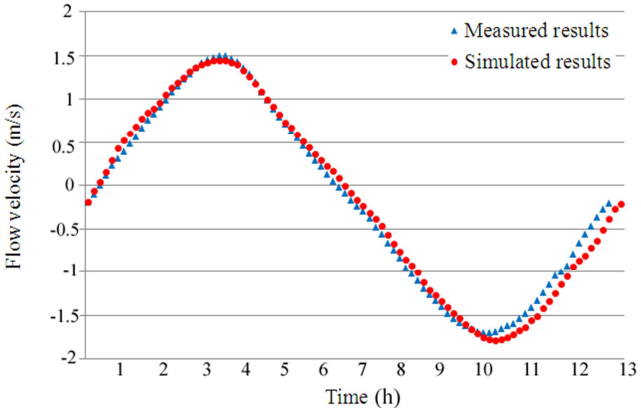


***Figure 5.*** *(Color online) Average velocity profiles obtained from field measurement and numerical simulation (The results were obtained at the centre of open channel).*

Percent difference in the two velocities is only 2.2%, which shows that the numerical simulation compares well with results of the field measurement.

### *6.3. The Best Scenario for Damming up*

As shown in all the tables and figures, the flow velocity and scoured depth increased almost linearly as the width of open channels decreased [10, 15, 19, 21, 30]. For all the scenarios, however, when the width of open channel was 50 m, the flow velocity and scoured depth increased very slightly than those in other widths. The result indicated that the width of 50 m is critical, namely, the flow velocity and scour depth in the open channels where the width is less than 50 m is not expected to increase any more. Also, when damming up according to scenario 1, the flow velocity and scoured depth in the open channels were smaller than those in other scenarios. As compared the flow velocity and scour depth according to all the scenarios, $V_{Scenario\,1} < V_{Scenario\,3} < V_{Scenario\,2}$ (where, $V$ is the maximum flow velocity in open channel), resulting in $SD_{Scenario\,1} < SD_{Scenario\,3} < SD_{Scenario\,2}$ (where, $SD$ is the maximum scour depth in open channel). The difference in the flow velocity and scour depth is due to dikes orienting at about 30° to the flow. The result suggested that scenario 1 is best for damming up. In other words, it is possible to economize on time, labor, and money for damming up.

## 7. Conclusions

In this study a hydrodynamic model for a final damming up area has been established and is capable of simulating water flows and scour depths in the open channels of a final damming up area. This model has been applied to a number of different scenarios for damming up in a tideland area. Because of some limitations of the 2-D numerical model the results are interpreted qualitatively. The numerical model has been validated by comparing the results with actual measurement. This in particular is very useful in determining hydrodynamic efficiency of different scenarios for damming up. The main effect of all the scenarios is clear. The numerical model has to be improved further for more reliable quantitatively results. Especially, a 3-D numerical model has to be studied further, considering improved stability and convergence, and shorter computational time, while achieving similar accuracy of obtained results.

## References


[1] Acharya, A. (2011) Experimental study and numerical simulation of flow and sediment transport around a series of spur dikes, *D. Sc. Thesis, The University of Arizona*.

[2] Afzal, M. S. (2013) 3D Numerical Modelling of Sediment Transport under Current and Waves, *M. S. Thesis, Norwegian University of Science and Technology*.

[3] Bakhtyar, R., Barry, D. A., Yeganeh-Bakhtiary, A. & Ghaheri, A. (2009) Numerical simulation of surf–swash zone motions and turbulent flow, *Advances in Water Resources*, 32, 250–263.

[4] Bihs, H. & Olsen, N. R. B. (2008) Three dimensional numerical modeling of pier scour, *In Fourth International Conference on Scour and Erosion, ICSE 4, Tokyo, Japan*.

[5] Bihs, H. & Olsen, N. R. B. (2011) Numerical modeling of abutment scour with the focus on the incipient motion on sloping beds, *Journal of Hydraulic Engineering*, 137 (10), 1287–1292.

[6] Cameron, S. M., Nikora, V. I. & Stewart, M. T. (2017) Very-large-scale motions in rough-bed open-channel flow, *J. Fluid Mech.*, 814, 416–429.

[7] Coleman, S. E., Lauchlan, C. S. & Melville, B. W. (2003) Clear-water scour development at bridge abutments, *Journal of Hydraulic Research*, 41 (5), 521–531.

[8] Comblen, R. et al. (2009) A finite element method for solving the shallow water equations on the sphere, *Ocean Modelling*, 28 (1–3), 12–23.

[9] Comer, J., Olbert, A. I., Nash, S. & Hartnett, M. (2017) Development of high-resolution multi-scale modelling system for simulation of coastal-fluvial urban flooding, *Nat. Hazards Earth Syst. Sci.*, 17, 205–224.

[10] Crnjaric-Zic, N., Vukovic, S. & Sopta, L. (2004) Balanced finite volume WENO and central WENO schemes for the shallow water and the open-channel flow equations, *Journal of Computational Physics*, 200 (2), 512–548.

[11] Daoud, A. H., Rakha, K. A. & Abul-azm, A. G. (2008) A two-dimensional finite volume hydrodynamic model for coastal areas: Model development and validation, *Ocean Engineering*, 35 (1), 150–164.

[12] Dawson, C. & Proft, J. (2004) Coupled discontinuous and continuous Galerkin finite element methods for the depth-integrated shallow water equations, *Computer Methods in Applied Mechanics and Engineering*, 193 (3–5), 289–318.

[13] Dey, S. (2003) Threshold of sediment motion on combined transverse and longitudinal sloping beds, *Journal of Hydraulic Research*, 41 (4), 405–415.

[14] Duc, B. & Rodi, W. (2008) Numerical simulation of contraction scour in an open laboratory channel. *Journal of Hydraulic Engineering*, 134 (4), 367–377.

[15] Dufresne, M. et al. (2010) Classification of flow patterns in rectangular shallow reservoirs. *Journal of Hydraulic Research*, 48 (2), 197–204.

[16] Guo, J. (2002) Hunter Rouse and Shields Diagram, *Advances in Hydraulic and Water Engineering*, 2, 1096–1098.

[17] Guo, W.-D., Hong, J.-H., Chen, C.-H., Su, C.-C. & Lai, J.-S. (2017) A Simplified Simulation Method for Flood-Induced Bend Scour – A Case Study Near the Shuideliaw Embankment on the Cho-Shui River, *water*, 9 (324), 1–19.

[18] Lu, C. N. & Li, G. (2011) Simulations of Shallow Water Equations by Finite Difference WENO Schemes with Multilevel Time Discretization, *Numerical Mathematics-Theory Methods and Applications*, 4 (4), 505–524.

[19] Meselhe, F. Sotiropoulos, & Jr (1997) Numerical Simulation of Transcritical Flow in Open Channels, *Journal of Hydraulic Engineering*, 123 (9), 774–783.

[20] Mortlock, T. R., Goodwin, I. D., McAneney, J. K. & Roche, K. (2017) The June 2016 Australian East Coast Low: Importance of Wave Direction for Coastal Erosion Assessment, *water*, 9 (121), 1–22.

[21] Mullin, T., Shipton, S. & Tavener, S. J. (2003) Flow in a symmetric channel with an expanded section, *Fluid Dynamics Research*, 33 (5–6), 433–452.

[22] Overduin, P. P., Wetterich, S., Günther, F., Grigoriev, M. N., Grosse, G., Schirrmeister, L., Hubberten, H.-W. & Makarov, A. (2016) Coastal dynamics and submarine permafrost in shallow water of the central Laptev Sea, East Siberia, *The Cryosphere*, 10, 1449–1462.

[23] Peng, Y., Zhou, J. G., & Burrows, R. (2011) Modelling the free surface flow in rectangular shallow basins by lattice Boltzmann method, *Journal of Hydraulic Engineering ASCE*, 137 (12), 1680–1685.

[24] Roulund, A., Sumer, B. M., Fredsøe, J., & Michelsen, J. (2005) Numerical and experimental investigation of flow and scour around a circular pier, *Journal of Fluid Mechanics*, 534, 351–401.

[25] Smith, H. D. (2004) Modeling the flow and scour around an immovable cylinder, *M. S. Thesis*, *Ohio State University*.

[26] Török, G. T., Baranya, S. & Rüther, N. (2017) 3D CFD Modeling of Local Scouring, Bed Armoring and Sediment Deposition, *water*, 9 (56), 1–23.

[27] Tubbs, K. R. & Tsai, F. T. C. (2011) GPU accelerated lattice Boltzmann model for shallow water flow and mass transport, *International Journal for Numerical Methods in Engineering*, 86 (3), 316–334.

[28] Vikas, S. (2005) Two dimensional sediment transport model using parallel computers, *M. S. Thesis*, *Banaras Hindu University*.

[29] Webster, T., McGuigan, K., Collins, K. & MacDonald, C. (2014) Integrated River and Coastal Hydrodynamic Flood Risk Mapping of the LaHave River Estuary and Town of Bridgewater, Nova Scotia, Canada, *Water*, 6, 517–546.

[30] Wu, W. (2004) Depth-Averaged Two-Dimensional Numerical Modeling of Unsteady Flow and Nonuniform Sediment Transport in Open Channels, *Journal of Hydraulic Engineering*, 130 (10), 1013–1024.

[31] Zhihe, Z. & Fernedo, H. J. S. (2007) Numerical Simulation of Scour around Pipelines Using an Eulerian-Eulerian Coupled Two-phase Model, *Journal of Fluid Mechanics*, 7, 121–142.

[32] Zhou, J. G. et al. (2001) The surface gradient method for the treatment of source terms in the shallow-water equations. *Journal of Computational Physics*, 168 (1), 1–25.

[33] Zhou, J. G. et al. (2002) Numerical solutions of the shallow water equations with discontinuous bed topography, *International Journal for Numerical Methods in Fluids*, 38 (8), 769–788.

[34] Zhou, J. G. (2011) Enhancement of the LABSWE for shallow water flows. *Journal of Computational Physics*, 230 (2), 394–401.